AEDC-TR-10-S-7

Comparison of Subpixel Phase Correlation Methods for Image Registration

R. A. Reed
Aerospace Testing Alliance

April 2010

Final Report for Period 1 October 2008 – 30 September 2009

Statement A: Approved for public release; distribution is unlimited.

ARNOLD ENGINEERING DEVELOPMENT CENTER
ARNOLD AIR FORCE BASE, TENNESSEE
AIR FORCE MATERIEL COMMAND
UNITED STATES AIR FORCE

NOTICES
When US Government drawings, specifications, or other data are used for any purpose other than a definitely related Government procurement operation, the Government thereby incurs no responsibility nor any obligation whatsoever, and the fact that the Government may have formulated, furnished, or in any way supplied the said drawings, specifications, or other data, is not to be regarded by implication or otherwise, as in any manner licensing the holder or any other person or corporation, or conveying any rights or permission to manufacture, use, or sell any patented invention that may in any way be related thereto.
Qualified users may obtain copies of this report from the Defense Technical Information Center.
References to named commercial products in this report are not to be considered in any sense as an endorsement of the product by the United States Air Force or the Government.

DESTRUCTION NOTICE

For unclassified, limited documents, destroy by any method that will prevent disclosure or reconstruction of the document.

APPROVAL STATEMENT

Prepared by:

ROBERT A. REED
Aerospace Testing Alliance

Reviewed by:

2LT GREGORY BOYADJIAN
Air Force Project Manager
718th Test Squadron

Approved by:

HULAND C. SMITH
Technical Director
718th Test Squadron

REPORT DOCUMENTATION PAGE	Form Approved OMB No. 0704-0188

PLEASE DO NOT RETURN YOUR FORM TO THE ABOVE ADDRESS

1. REPORT DATE (DD-MM-YYYY)	2. REPORT TYPE	3. DATES COVERED *(From – To)*
xx-04-2010	Final Report	1 Oct 2008 – 30 Sep 2009

4. TITLE AND SUBTITLE	5a. CONTRACT NUMBER
Comparison of Subpixel Phase Correlation Methods for Image Registration	5b. GRANT NUMBER
	5c. PROGRAM ELEMENT NUMBER
6. AUTHOR(S)	5d. PROJECT NUMBER
Reed, Robert. A.	10909
	5e. TASK NUMBER
	5f. WORK UNIT NUMBER

7. PERFORMING ORGANIZATION NAME(S) AND ADDRESS(ES)	8. PERFORMING ORGANIZATION REPORT NO.
Aerospace Testing Alliance, Arnold Air Force Base, TN 37389	AEDC-TR-10-S-7
9. SPONSORING/MONITORING AGENCY NAME(S) AND ADDRESS(ES)	10. SPONSOR/MONITOR'S ACRONYM(S)
Arnold Engineering Development Center Arnold AFB, TN 37389	11. SPONSOR/MONITOR'S REPORT NUMBER(S)

12. DISTRIBUTION/AVAILABILITY STATEMENT

Statement A: Approved for public release; distribution is unlimited.

13. SUPPLEMENTARY NOTES

Available in the Defense Technical Information Center (DTIC).

14. ABSTRACT

The popular phase correlation method (PCM) for image registration has been extended to subpixel accuracy by several alternative algorithms, each claiming accuracies on the order of 0.02 – 0.03 pixels for 256 x 256 images. However, the performance reported in the literature is sometimes based upon idealized images or upon just a few selected images. This leaves users in doubt as to which algorithm is truly superior. This work compares three subpixel PCM algorithms using a common test set of realistic images derived from satellite imagery. Of the three algorithms investigated in this work, the one of Guizar et al. (conceptually the simplest) consistently performed best.

15. Subject Terms

Frame registration, phase correlation method, PCM, image processing

16. SECURITY CLASSIFICATION OF:			17. LIMITATION OF ABSTRACT	18. NUMBER OF PAGES	19A. NAME OF RESPONSIBLE PERSON
A. REPORT	B. ABSTRACT	C. THIS PAGE			Robert A. Reed
Unclassified	Unclassified	Unclassified	Same as Report	11	19B. TELEPHONE NUMBER *(Include area code)* (931) 454-4648

CONTENTS

FIGURES

TABLES

1.0 INTRODUCTION

When working sequences of images, registration of the frames to a common point of reference is an essential prerequisite for many types of image analysis. Examples include

- Coadding images to improve signal-to-noise ratio (SNR)
- Superresolution
- Color ratios
- Polarization ratios
- Pan-sharpening
- Conversion of infrared multispectral imagery to emissivity-temperature space

Example – This section begins with an example showing the importance of accurate frame registration. Figure 1 shows an IKONOS satellite image of Venice. The color ratio of an image is frequently used for classification in multispectral imagery. The green vs. red color ratio for this image was computed by extracting the green and red components of the image and performing simple element-by-element matrix division (R1 = Green/Red). The color ratio was computed a second time (R2) using a green image with a (deliberate) subpixel registration error of 0.1 pixel. Figure 2 displays the quantity (R2-R1)/R1, which is the normalized error in color ratio. Although the registration error is small, the color ratio error is as large as 15%. This sensitivity to frame registration is typical for many image analysis procedures. Therefore, it is important to choose the best frame registration technique available.

Figure. 1. IKONOS Image of Venice

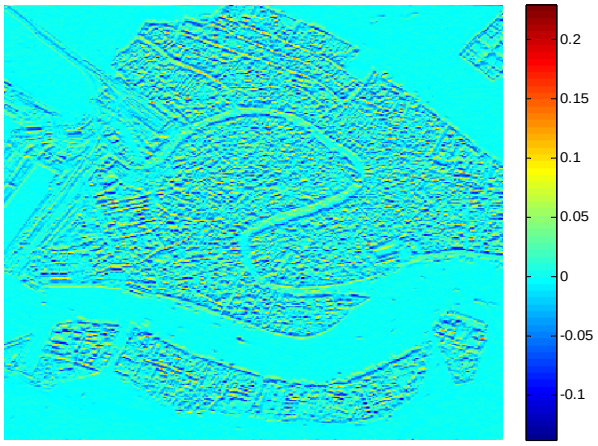

Figure. 2. Error in Color Ratio

2.0 PHASE CORRELATION METHOD

The phase correlation method[1-2] (PCM) is a popular Fourier domain method to register two images. It computes a phase difference map that (ideally) contains a single peak. The location of the peak is proportional to the relative translation [dx, dy] between the two images. The PCM is resilient to noise and image defects and is readily automated. It is completely equivalent to

correlation in the spatial domain, but the calculation is orders of magnitude faster in the Fourier domain. The mathematical details are as follows:

Consider two identical images i1 and i2, with i2 shifted by an amount [Δx, Δy] relative to i1,

$$i2(x,y) = i1(x-\Delta x, y-\Delta y) \tag{1}$$

and which obey periodic boundary conditions,

$$i1(M+x, N+y) = i1(x,y) \tag{2}$$

where the image size is MxN pixels. Denote Fourier transforms of i1 and i2 by I1 and I2. From the Fourier shift theorem, I1 and I2 differ only by a linear phase term $j(\omega_x\Delta x + \omega_y\Delta y)$. Specifically,

$$I2(\omega_x, \omega_y) = I1(\omega_x, \omega_y)\, e^{j(\omega_x \Delta x + \omega_y \Delta y)} \tag{3}$$

where ω_x and ω_y are the frequency variables in column and row. The normalized cross-power spectrum of the images C12 is defined as

$$C12(\omega_x, \omega_y) = \frac{I1.*conj(I2)}{\left|I1.*conj(I2)\right|} = e^{-j(\omega_x \Delta x + \omega_y \Delta y)} \tag{4}$$

The operator * is the Schur product (also known as the Hadamard element-by-element matrix product) and conj is the complex conjugate operator. The right-hand side of Eq. (4) is simply the Fourier transform of a Dirac delta function. Stated differently, the inverse Fourier transform of the normalized cross-power spectrum C12 is a two-dimensional Dirac delta function δ(x-Δx) δ(y-Δy) with a peak location corresponding to the displacement [Δx, Δy] between the two images (Fig. 3). Leprince et al.[1] show that this result remains unbiased in the presence of additive noise or optical blur. The inset in the upper right-hand corner of the phase map shows that for real images, which contain both noise and uncorrelated content, the peak is distorted from the ideal delta function profile.

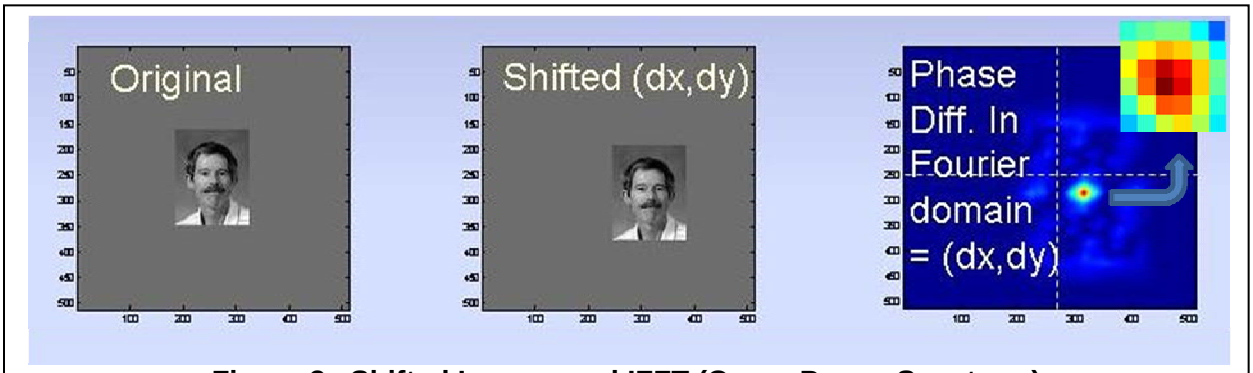

Figure 3. Shifted Images and IFFT (Cross-Power Spectrum)

3.0 ACCURACY TRADE-OFFS

The accuracy of PCM registration depends upon the content and quality of the images. Representative trade-offs of accuracy vs. image noise and array size are indicated in this section. Perhaps the most prominent advantage of the PCM is that it is exceptionally robust against noise. The accuracy of the PCM for the clean image on the left of Fig. 4 is 0.02 pixels. For the severely degraded noisy image on the right of Fig. 4 (11% rms noise), the registration accuracy is still 0.15 pixels. Considering the poor quality of the image, this level of accuracy is truly remarkable. The accuracy for variable rms noise levels is shown in Fig. 5. The rms noise level in Fig. 5 is given in counts, and the image itself has a dynamic range of 8 bits (0 to 255 counts). Figure 6 shows that, as expected, the registration accuracy improves for larger images. The abscissa is the linear dimension of the (square) focal plane array in pixel units.

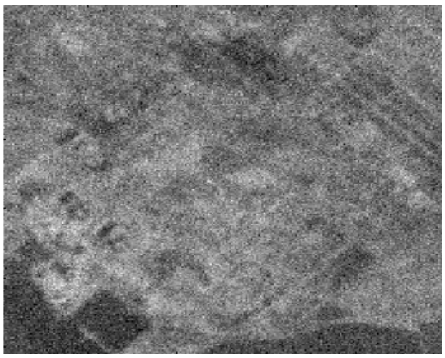

Figure 4. Original vs. Degraded Noisy Image.

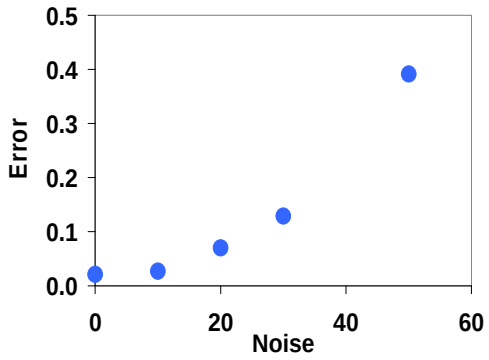

Figure 5. Error vs. Noise

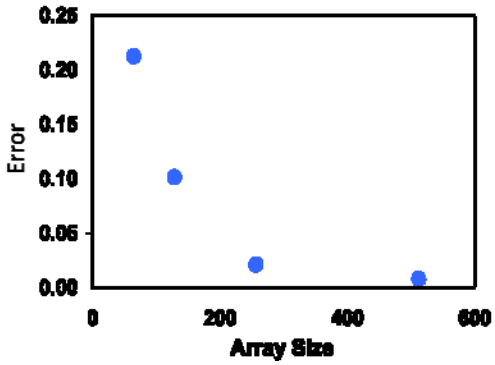

Figure 6. Error vs. Array Size

Periodic Boundary Conditions vs. the Real World – An essential feature of the present work is that it uses realistic images that do not obey periodic boundary conditions. The PCM is strictly applicable to images that obey periodic boundary conditions (Eq. [2]). However, images of this kind are unphysical. Figures 7 and 8 illustrate the unphysical "world view" according to periodic boundary conditions. In this "world view," the original frame repeats endlessly like a mosaic. A shifted image (e.g., denoted by the dashed line) contains exactly the same features as the original image. The only difference is that the spatial features have been cyclically shifted (Fig. 9). The result is that the shifted frame can be brought into perfect correlation with the original one by a simple cyclic "unshift" of the shifted frame. However, periodic boundary conditions hardly

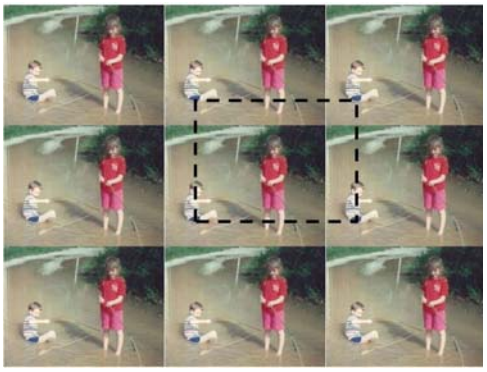

Figure 7. Periodic Boundary Conditions

Figure 8. Image Shifted According To Periodic Boundary Conditions

ever apply in the real world. Thus a fundamental assumption (Eq. [2]) underlying the PCM is hardly ever obeyed by any pair of real images.

Figure 9. True Shifted Images

The correct "world view" for two shifted frames is illustrated by the yellow and red outlined frames in Fig. 9. Each image is a different sample taken from the same global scene. The two images share a great deal of common features. These are useful for correlation, which is at the heart of the PCM. However, each frame also contains features near the edge that the other does not share. For example, the boy is entirely within the image denoted by the red frame, but only partially within the image denoted by the yellow frame. These uncorrelated features inject noise into the PCM correlation. This in turn sets a fundamental limit on the accuracy of frame registration. If the images are decomposed into correlated vs. uncorrelated parts:

$$I1 = I1^{C} + I1^{U} \tag{5}$$

$$I2 = I2^{C} + I2^{U} \tag{6}$$

then Eq. (4) for the normalized cross-product will deviate from the ideal case (delta function) by a factor proportional to the fraction of the image that is uncorrelated.

$$Error \cong \left| \frac{I^{U}}{I^{C}} \right| \cong \frac{Area\,of\ uncorrelated\ image}{Area\,of\ correlated\ image} \tag{7}$$

This is an intuitively reasonable result.

In order to be realistic, the test images used in this work were all generated according to the procedure illustrated in Fig. 9. Specifically, all shifted images were selected from a larger global scene and contain uncorrelated content near the borders (i.e., as actually happens in the real world). They were not generated by cyclic shifting with periodic boundary conditions. This

ensures that the performance estimates provided in this work are representative of the performance one will actually obtain on real-world images – none of which obey periodic boundary conditions. The PCM works in practice because when the shift between the two images is small compared to the size of the image, most of the scene is common to both frames. Therefore, correlation still works fairly well. In addition, uncorrelated effects at the borders of the images are mitigated by multiplying each image by a window function that smoothly tapers to zero at the edges of the image.

Test Images – In addition to nonperiodic boundary conditions, real images are subject to noise and frequency aliasing. In addition, some focal plane arrays have dead space between the pixels. If one is concerned with registering images to within only ±1 pixel, these real-world effects are generally inconsequential. However, they become significant as one attempts to push the PCM to subpixel accuracy. Therefore, the test images used to determine algorithm performance contain all of these real-world effects. The test images used in this investigation (Fig. 10) were derived from high-resolution (approx 3,000 x 3,000 pixels) satellite images of terrestrial scenes. The images included diverse scenes – ocean, urban, desert, and rural. Downsampled shifted images, such as would be observed by a lower resolution sensor, and containing the aforementioned "real-world" effects, were generated as follows. The original high-resolution satellite image was first blurred by a Gaussian point-spread function (PSF) to simulate the optics blur of the sensor. The blurred image was then downsampled by a factor of 10 onto a rectilinear focal plane array (FPA) of size NFPA x NFPA, as notionally indicated in Fig. 11. The baseline value was NFPA = 256 pixels. The aimpoint of the FPA with respect to the (blurred) high-resolution image was offset by integral pixel amounts, as measured in the high spatial resolution coordinate system. Thus, after downsampling, the image shifts were exact

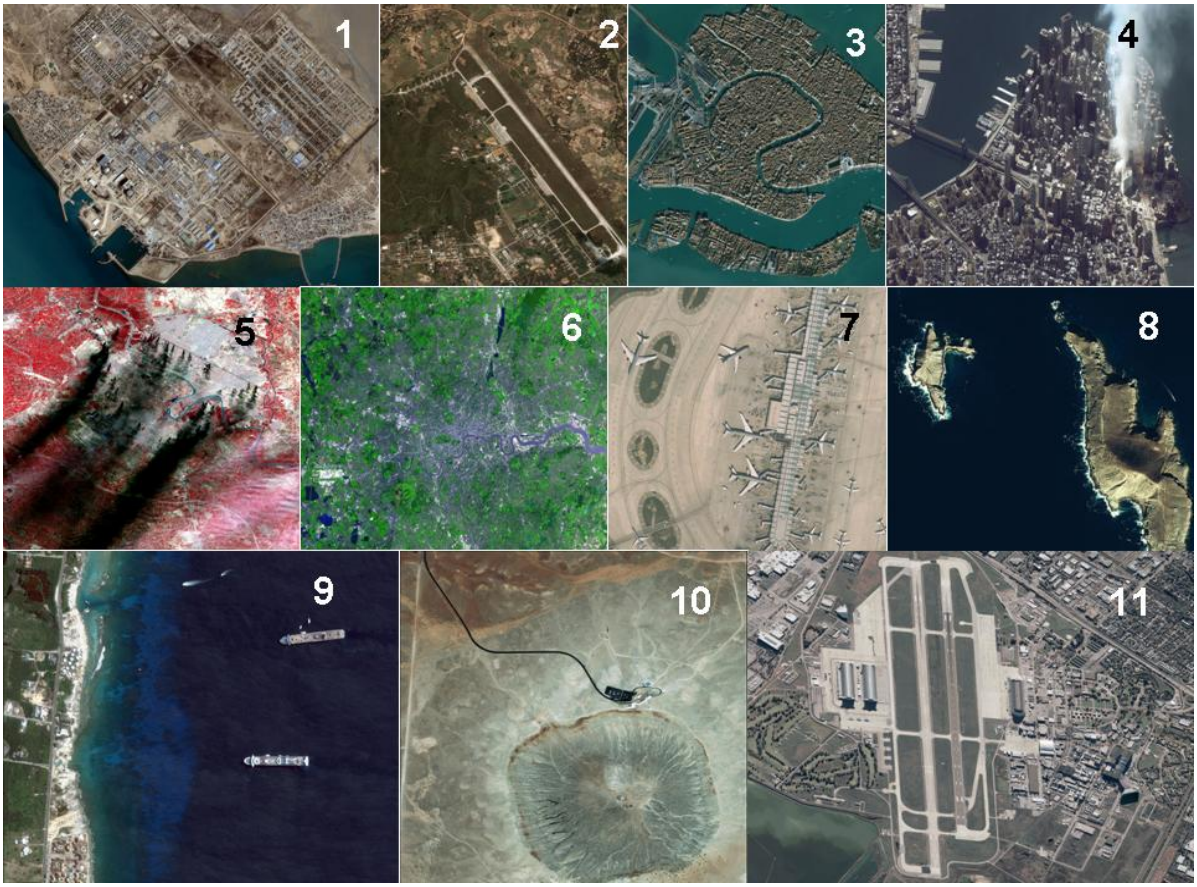

Figure 10. Test Images (Before Blurring)

multiples of 0.1 pixel. Each pixel of the simulated FPA was surrounded by an optional inactive dead space to simulate a fill factor < 100%. (The fill factor of a sensor array is the ratio of active area to total area.) The nominal fill factor was 0.8^2 = 64%. Gaussian additive noise was added as the last step in the simulation. A Gaussian blur kernel was used, so the downsampled images have a realistic amount of aliasing.

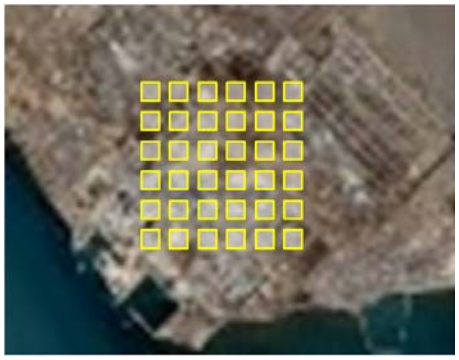

Figure 11. Sensor Simulation (Actual Simulation Uses 256 x 256 Array)

Description of Algorithms - Method 1 by Hoge[3] uses singular value decomposition (SVD) to isolate the dominant rank-one principal component of the phase difference matrix. This method was developed for magnetic resonance imaging. Method 2 by Ren, Vlachos, and Jiang[4] (RVJ) uses a subspace projection method to fit a linear function (i.e., a plane) to the phase of the normalized cross-power spectrum (Eq. [4]). It is the fastest of the three methods. Method 3 by Guizar-Sicairos, Thurman, and Fienup[5] (GTF) is a traditional PCM approach with a Discrete Fourier Transform interpolation routine to accurately determine the peak location with small memory allocation. Each of these methods has specific strengths that, if combined into a single code, might possibly outperform any of the individual methods. However, this was beyond the scope of this report. Method 3 turned out to be the most reliable, so two variants of Method 3 were investigated in an effort to achieve even better accuracy. Method 4 applies a complex gradient operator to the images[6] before applying Method 3. Specifically, the original image, I, was replaced by the complex gradient image, I_{CG}. This operation acts as a high-pass filter to enhance edges and high spatial frequencies.

$$I_{CG} = \left\{ \frac{\partial}{\partial x} + i \frac{\partial}{\partial y} \right\} I \tag{6}$$

Method 5 applies histogram equalization to the images before applying Method 3.

Results – This section describes the accuracies of the three registration methods (plus the two variants of Method 3) based upon the 11 test images of Fig. 10. The baseline conditions were a square focal plane with dimension NFPA = 256 pixels, dynamic range = 8 bit, 10 counts rms additive Gaussian noise, and FPA fill factor = 64%. For all methods, the downsampled images were apodized by a cosine window function before attempting frame registration. Foorosh et al.[7] recommend prefiltering of the phase difference matrix to remove aliased components (generally at high spatial frequencies). This recommendation was not implemented in the present investigation, but it is a good idea that should increase the accuracy of any subpixel PCM algorithm. The difficulty is that the filtering must be tailored to each image and sensor.

Figure 12 and Table 1 show the registration accuracy for Methods 2 through 5. Method 3 (GTF) and its two minor variants (Methods 4 and 5) performed best. The performance of Method 2 (RVJ) was comparable to that of Method 1 (GTF) for 8 out of the 11 images. However, it was noticeably poorer for image Nos. 1, 7, and 10. The author could find nothing special about these three images to explain why the algorithm of Method 2 performed poorly in these particular cases. Method 1 (Hoge) performed poorly for optical imagery, and the results are not shown in Fig. 12. Minor improvements to the accuracy of Method 3 were achieved by preprocessing according to Methods 4 and 5. Figure 13 shows the robustness vs. additive Gaussian noise

(rms counts). Method 2 was the first to "break" (at 50 counts rms noise) under the load of increasing noise. This is an extremely high noise level and would not likely be encountered in practice.

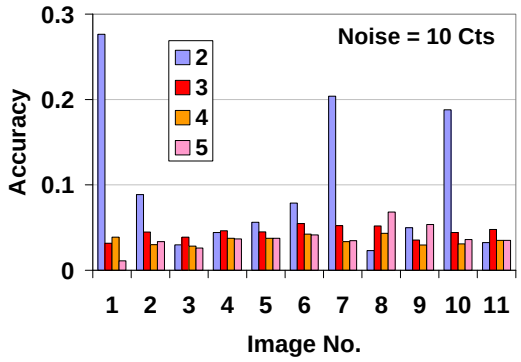

Figure 12. Registration Accuracy

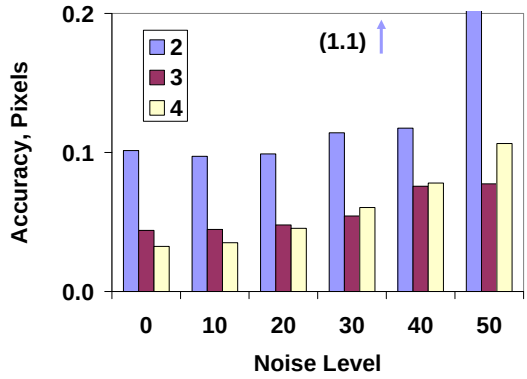

Figure 13. Noise Sensitivity

Method	1	2	3	4	5
Mean	1.210	0.097	0.045	0.035	0.038
StdDev	0.982	0.086	0.007	0.005	0.014

Table 1. Registration Accuracy of Various Methods

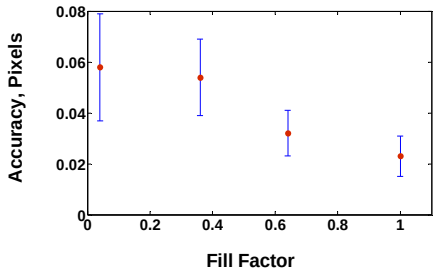

Figure 14. Fill Factor Effect

Figure 14 displays the registration accuracy of Method 4 vs. the FPA fill factor. The noise level was set to zero for this study. The fill factor introduces a small error into the frame registration process. This point has not been mentioned in the literature.[1-7]

SUMMARY

A reliable algorithm for subpixel accuracy frame registration is needed to accurately process multispectral imagery. Three different extensions of the popular PCM (phase correlation method) to subpixel frame registration were evaluated using a common set of satellite images. The test images derived from the satellite images include real-world effects such as nonperiodic boundary conditions, dead space between pixels, and additive noise. The results are as follows:

1. Algorithm Comparison:

    - Method 3 (GTF) and its two minor variants (Methods 4 and 5) performed best, with registration errors consistently on the order of 0.05 pixels or less. This registration accuracy pertains to 256 x 256 images with rms noise levels as high as 10%.

- Method 2 (RVJ) performed inconsistently. It worked as well as Method 3 for most images, but poorly for others.

- Method 1 (Hoge) is not recommended in its present form. However, the mathematical basis is sound, and with minor changes it might be made to perform as well as the other methods.

2. Insignificant Gains from Preprocessing:

   Attempts to further increase the accuracy of registration by preprocessing the images (e.g., by taking gradients or by performing histogram equalization of the intensities) led to only minor gains in accuracy.

3. Effect of Focal Plane Array (FPA) Fill Factor

   The fill factor of the FPA sets a limit upon the achievable accuracy. However, this effect will generally be only a small part of the error budget for most imaging systems.

REFERENCES

1. Leprince, S., Barbot, S., Ayoub, F., and Avouac, J. P., "Automatic and Precise Orthorectification, Coregistration, and Subpixel Correlation of Satellite Images, Application to Ground Deformation Measurements," IEEE Trans. Geoscience Remote Sensing Vol. 45, No. 6, June 2007, pp. 1,529-1,558.

2. Stone, H., Orchard, M., and Chang, E. C., "Subpixel Registration of Images," in *Rec. 33rd Asilomar Conf. Signals, Systems, and Computers*, Vol. 2, 1999, pp. 1,446–1,452.

3. Hoge, W. S., "A Subspace Identification Extension to the Phase Correlation Method," IEEE Transactions on Medical Imaging, Vol. 22, No. 2, Fed 2003, pp. 277-280.

4. Ren, Jinchang, Vlachos, Theodoe, and Jiang, Jianmin, "Subspace Extension to Phase Correlation Approach for Fast Image Registration," Proceedings of the International Conference on Image Processing, ICIP 2007, 16-19 September 2007, San Antonio, TX, USA. ICIP (1) 2007: 481-484.

5. Guizar-Sicairos, Manuel, Thurman, Samuel T., and Fienup, James R., "Efficient Subpixel Image Registration Algorithms," OPTICS LETTERS, Vol. 33, No. 2, 15 January 2008, pp. 156-158.

6. Homblot, F., Collin, B., and Mohammad-Djafari, A., "Evaluation and Practical Issues of Image Registration Using Phase Correlation Methods," Proc. PSIP2005, 31 Jan – 2 Feb 2005, Toulouse, France.

7. Foroosh, H., Zerubia, J. B., and Berthod, M., "Extension of Phase Correlation to Subpixel Registration," *IEEE Trans. Image Processing*, Vol. 11, pp. 188-200, March 2002.